
DeblurDiff: Real-World Image Deblurring with Generative Diffusion Models

Lingshun Kong^{1,2*} Jiawei Zhang² Dongqing Zou^{2,3} Jimmy Ren² Xiaohe Wu⁴ Jiangxin Dong¹ Jinshan Pan¹
¹ Nanjing University of Science and Technology ² SenseTime Research ³ PBVR ⁴ Harbin Institute of Technology

Abstract

Diffusion models have achieved significant progress in image generation. The pre-trained Stable Diffusion (SD) models are helpful for image deblurring by providing clear image priors. However, directly using a blurry image or pre-deblurred one as a conditional control for SD will either hinder accurate structure extraction or make the results overly dependent on the deblurring network. In this work, we propose a Latent Kernel Prediction Network (LKPN) to achieve robust real-world image deblurring. Specifically, we co-train the LKPN in latent space with conditional diffusion. The LKPN learns a spatially variant kernel to guide the restoration of sharp images in the latent space. By applying element-wise adaptive convolution (EAC), the learned kernel is utilized to adaptively process the input feature, effectively preserving the structural information of the input. This process thereby more effectively guides the generative process of Stable Diffusion (SD), enhancing both the deblurring efficacy and the quality of detail reconstruction. Moreover, the results at each diffusion step are utilized to iteratively estimate the kernels in LKPN to better restore the sharp latent by EAC. This iterative refinement enhances the accuracy and robustness of the deblurring process. Extensive experimental results demonstrate that the proposed method outperforms state-of-the-art image deblurring methods on both benchmark and real-world images. The codes will be released in: <https://github.com/kkk1s/DeblurDiff>.

1. Introduction

Image deblurring aims to recover a sharp image from a blurry observation. Blurring can be caused by various factors, such as camera shake and high-speed movement of

the photographed objects. This task is challenging as only the blurry images are available and the blur might be non-uniform. Traditional deblurring methods (Pan et al., 2017; 2016) have made significant progress by utilizing hand-crafted features and priors. However, these methods often struggle to handle complex blur patterns and may produce unsatisfactory results. Recently, numerous learning-based approaches (Tao et al., 2018; Cho et al., 2021; Zamir et al., 2021; Chen et al., 2022) have been inclined to employ a variety of convolutional neural network (CNN) architectures. Compared with traditional algorithms, CNNs have demonstrated remarkable success. However, convolution operation is a spatially invariant local operation, which cannot effectively model the spatially variant characteristics of image content and the global contexts for image deblurring. STAFN (Zhou et al., 2019) employs a Kernel Prediction Network (KPN) to estimate a spatially variant kernel to assist with deblurring. To address the limitations of CNNs, Transformers (Zamir et al., 2022; Wang et al., 2022; Li et al., 2023; Kong et al., 2023) have been increasingly applied to image deblurring and have achieved commendable performance.

However, the above regression-based methods, which often use L2 and L1 reconstruction losses, tend to predict the mean rather than a plausible high-resolution (HR) solution (Lugmayr et al., 2020). This results in overly smooth outputs, leading to a significant loss of detail. To address this problem, recent methods (Kupyn et al., 2018; 2019; Ledig et al., 2017; Pan et al., 2021) have adopted adversarial training and perceptual loss functions to generate more detailed results. However, generative adversarial networks (GANs) suffer from training instability, mode collapse, and limited diversity in complex data generation, which may hinder the plausibility of the generated images.

Recently, diffusion models have demonstrated outstanding performance in image generation (Ho et al., 2020; Dhariwal & Nichol, 2021). Some researchers have attempted to utilize Denoising Diffusion Probabilistic Models (DDPMs) for image restoration (Ren et al., 2023; Yue et al., 2024), aiming to leverage their ability to capture complex data distributions and generate detailed images. However, due to the lack of large-scale pre-training, these methods have not demonstrated satisfactory results, particularly when applied

* This work was done during an intern at Sensetime Research.

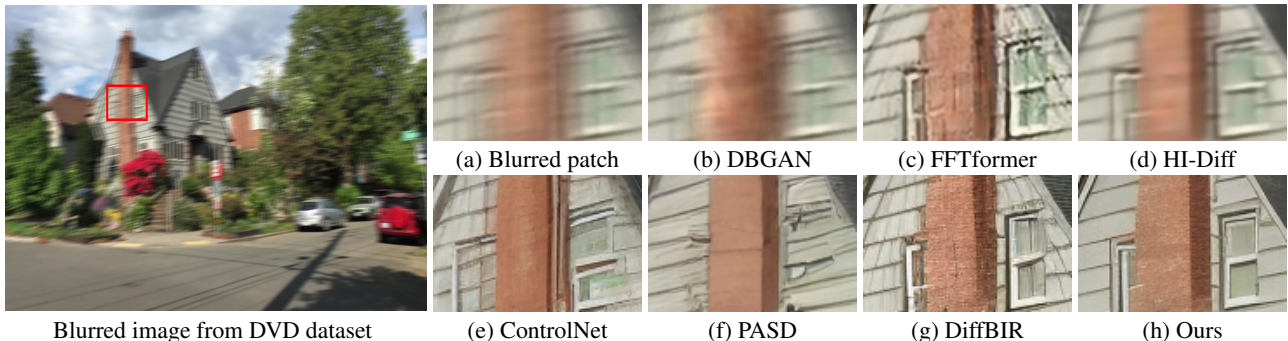


Figure 1. Visual comparison with state-of-the-art image deblurring methods. The results of GAN-based method (b) and diffusion-based method without pretraining (d) still contain significant blur effects. Directly using the blurry image as the conditional input (e) presents significant challenges in effectively extracting structural information. (f) is a method based on pre-trained SD that performs pre-deblurring on the input features, which alters the original information, leading to erratic generation. For (g), it uses the result of the pre-trained FFTformer (c) as the condition. (g) is influenced by the erroneous structures in (c), resulting in generated outputs that retain erroneous artifacts and erroneous structures. In contrast, our approach, guided by the clear structural information provided by LKPN, generates a more distinct and artifact-free image.

to out-of-distribution data, often leading to inferior performance and visually unpleasant artifacts. With the surprising performance of large-scale pre-trained models like Stable Diffusion (SD) in image generation, it has been developed for image restoration (Lin et al., 2025; Yang et al., 2024). SD models have strong priors on the structure and details of high-quality (HQ) images. However, directly utilizing blurry images as conditional inputs can hinder the extraction of effective structural information, especially in cases of severe blur, ultimately resulting in inaccurately generated structures (Figure 1(e)). While recent methods attempt to mitigate these limitations, their technical trajectories introduce new issues. These methods (Lin et al., 2025; Yang et al., 2024) require training an additional Degradation Removal Model (DRM) to first restore the clear images, and then enhance the details using a ControlNet (Zhang et al., 2023). This suggests that the restoration results of the entire method are notably influenced by the results of the degradation removal model. When the DRM (implemented via FFTformer (Kong et al., 2023)) yields inaccurate results (Figure 1 (c)), it may adversely affect the diffusion process, potentially resulting in suboptimal performance (Figure 1 (g)). Moreover, due to the poor generalization of existing degradation removal models across different datasets, these methods also tend to perform poorly when dealing with various types of blur.

In this paper, we investigate in-depth the problem of how to leverage pre-trained SD models to assist in real-world image deblurring while reconstructing realistic details and textures. This approach circumvents the direct use of blurry images as conditions, as severe blur can hinder the extraction of accurate structural information, leading to suboptimal final generated structures. Unlike pre-training an additional degradation removal model, which uses restored images as conditions and can be problematic due to poor restoration quality introducing incorrect structures and resulting

in erroneous generation, we jointly train a Latent Kernel Prediction Network (LKPN) with the diffusion model. The LKPN, together with EAC, is designed to guide the conditional generation at each step of the diffusion process.

The effectiveness of the LKPN lies in its ability to predict dedicated convolution kernels for each latent pixel, dynamically adjusting the kernel weights based on local content (e.g., edges, textures, and flat regions). These pixel-specific kernels are then applied to the latent blurry image by the element-wise adaptive convolution (EAC), enabling better restoration of clear structures by adaptively addressing distinct blur characteristics at each latent pixel location. This adaptive mechanism not only preserves the necessary information in the input image but also avoids the destruction of structural details, making it particularly advantageous for recovering fine structures and textures. By integrating the LKPN, the diffusion model uses the clear structures from the LKPN as conditional inputs to guide its generation process at each step. This produces more accurate results and enhances both deblurring and detail reconstruction. Furthermore, the intermediate results obtained at each step of the diffusion process are utilized to refine the output of the LKPN, progressively improving the accuracy of the deblurred results by EAC. This iterative refinement generates increasingly clearer conditional inputs, which in turn guide the generation process of the Stable Diffusion (SD) model to achieve iterative improvements. Additionally, the LKPN continuously benefits from the strong prior structures and detailed information provided by SD, enabling it to estimate better kernels to remove blur in latent space.

The main contributions are summarized as follows:

- We are the first to design an architecture based on pre-trained SD models to achieve effective deblurring while reconstructing realistic details and textures.
- We propose an LKPN architecture that estimates a

spatially variant kernel, which is then utilized by the EAC to progressively generate clear structures and preserve the necessary information in the input image throughout the diffusion process. This guides SD to produce more accurate details and structures, thereby enhancing the overall deblurring performance.

- We quantitatively and qualitatively evaluate the proposed method on benchmark datasets and real-world images and show that our method outperforms state-of-the-art methods.

2. Related Work

Image deblurring. Due to the fact that image deblurring is an ill-posed problem, traditional methods (Krishnan et al., 2011; Pan et al., 2017; 2016) often develop various effective priors to constrain the solution space. These manually designed priors can help remove blur. However, they do not fully utilize the characteristics of clear image data, which leads to a struggle in handling complex blur patterns and may produce unsatisfactory results

With the development of deep learning, many learning-based methods have tended to use various CNN architectures for image deblurring. SRN (Tao et al., 2018) proposes a multi-scale structure that performs image deblurring from coarse to fine. MIMOUnet (Cho et al., 2021) redesigns the coarse-to-fine structure, significantly reducing the computational cost. NAFNet (Chen et al., 2022) analyzes the baseline module and simplifies it by removing the activation function, which better facilitates image restoration.

Due to the excellent performance of Transformers in global context exploration and their great potential in many visual tasks, some methods have applied it to image deblurring. Restormer (Zamir et al., 2022) simplifies the baseline module by estimating self-attention in the channel dimension, reducing the computational cost of self-attention Uformer (Wang et al., 2022) proposes a general U-shaped Transformer model, computing self-attention within local windows to address the image deblurring. FFTformer (Kong et al., 2023) proposes a frequency-domain based Transformer model and achieved state-of-the-art results.

Although these methods have achieved good deblurring effects, these regression-based methods tend to predict smooth results, with limited ability to depict details.

Diffusion model. Denoising Diffusion Probabilistic Models (DDPM) (Ho et al., 2020) have shown remarkable capabilities in generating high-quality natural images. Some methods (Yue et al., 2024; Ren et al., 2023; Chen et al., 2023) have attempted to directly train a diffusion model for image restoration. Rombach et al. (Rombach et al., 2022)

extended the DDPM structure to the latent space and conducted large-scale pre-training, demonstrating impressive generative capabilities. Recently, some researchers have utilized powerful pre-trained generative models, such as SD (Rombach et al., 2022), to address image restoration problems. DiffBIR (Lin et al., 2025) proposes a two-stage approach, first restoring the degraded image and then using SD to generate details. PASD (Yang et al., 2024) restores clear images through a Degradation Removal module to provide clear conditional inputs for SD.

However, these methods require training an additional image restoration model and then enhance the details through SD. This means that the final results of the SD largely depend on the outcomes of the restoration model. When the degradation removal model produces erroneous results, it may lead to poor performance in the diffusion process. Moreover, due to the poor generalization of existing restoration models, these methods also tend to perform poorly when dealing with various types of blur.

3. Method

Our goal is to leverage the powerful priors of pre-trained Stable Diffusion models to achieve robust image deblurring, while simultaneously reconstructing realistic details and textures. Specifically, we introduce a framework that integrates a Latent Kernel Prediction Network (LKPN) with the diffusion process. The LKPN estimates pixel-specific kernels in the latent space, enabling adaptive deblurring tailored to the distinct characteristics of each pixel. By iteratively refining the deblurred results throughout the diffusion process, our approach progressively restores clear structures and enhances fine details. Figure 3 shows the overview of the proposed method.

3.1. Motivation and Preliminaries

Motivation. Directly using the blurry image as the condition of SD leads to suboptimal deblurring, as it lacks sufficient structural information to effectively guide the generation process, making it difficult for diffusion models to recover clear structures and details as shown in Figure 2(c). When using a pre-trained network to process the blurry image, if the deblurring result is inaccurate, it can introduce incorrect structures (Figure 2(b)). This, in turn, leads to the diffusion model generating erroneous structures during its iterative process (Figure 2(d)). In this paper, we utilize the image priors from Stable Diffusion (SD) and the blurry image together to help us predict an accurate clear structure, thereby more accurately guiding the generation process.

Our work is motivated by existing methods (Yuan et al., 2007; Zhao et al., 2024), which have explored using paired noisy and blurry images to improve deblurring performance.

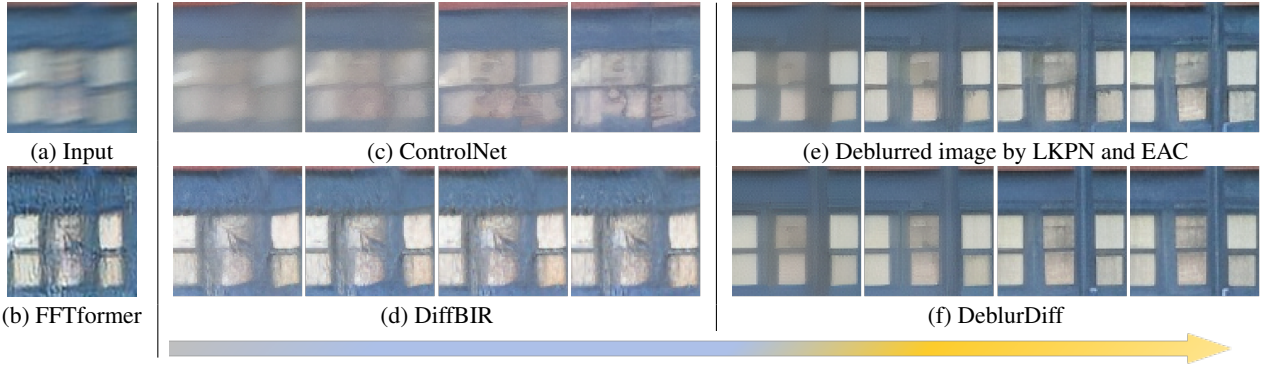


Figure 2. Iterative results of the diffusion model. The arrow represents the iterative diffusion process. To visualize this process, we decode the features deblurred by the LKPN and EAC to the image space using the VAE decoder in each time step. Using the blurry image directly as a conditional input (c) makes the diffusion model struggle to recover clear structures and fine details in (a). For (d), it uses the result of the pre-trained FFTformer (b) as the condition. However, the deblurring network can introduce incorrect structures, leading to erroneous content generation. In contrast, the proposed LKPN can preserve the input information and restore the structure (e) by EAC, thereby guiding the diffusion model to generate better results (f).

However, obtaining paired images is often quite difficult in practical applications, which limits the applicability of these methods. In contrast, our approach leverages the intermediate noise representations generated during the diffusion process to guide deblurring. Our method generates a guidance with clear structures during the diffusion process (Figure 2(e)), enabling the diffusion model to produce clearer and more accurate results while retaining more of the input information as shown in Figure 2(f).

Denosing Diffusion Probabilistic Models (DDPM) are a type of probabilistic model that learn the data distribution $p(x)$ by progressively denoising a normally distributed variable. The training process involves a forward noise-adding process and a reverse denoising process. At the t -th step of the forward diffusion process, a noisy image x_t is generated from the clear image x_0 by:

$$x_t = \sqrt{\bar{\alpha}_t}x_0 + \sqrt{1 - \bar{\alpha}_t}\epsilon, \quad (1)$$

where ϵ denotes the noise sampled from the standard normal distribution $\mathcal{N}(0, I)$, and $\bar{\alpha}_t$ controls the amount of noise added at each step t , which is typically a predefined value. In the reverse denoising process, a denoising neural network $\epsilon_\theta(x_t, t)$ is used to predict the noise in x_t . After training, the denoising network can iteratively run for T steps starting from noise sampled from a standard normal distribution to generate a clear image. To improve computational efficiency, the diffusion process is often transferred from the pixel space to the latent space, where high-frequency, imperceptible details are abstracted away via a pre-trained Variational Autoencoder (VAE). This latent space is more suitable for likelihood-based generative models as it focuses on the important and semantic parts of the data, operating in a lower-dimensional and computationally efficient space (Rombach et al., 2022). Specifically, a pre-trained VAE is utilized to transform the clear image x_0 into a latent representation z_0 by $z_0 = \mathcal{E}(x_0)$, and the forward noising

and reverse denoising processes of DDPM are performed in this latent space. The corresponding optimization objective can be simplified to minimizing the denoising loss:

$$\mathcal{L}_{\text{denoise}} = \mathbb{E}_{z_t, \epsilon \sim \mathcal{N}(0, I), t} \left[\|\epsilon - \epsilon_\theta(z_t, t)\|_2^2 \right]. \quad (2)$$

where z_t is the noisy latent representation at step t .

3.2. LKPN for clear structure guidance.

In the context of blind deblurring, directly using blurry images as conditions can impede the extraction of effective structural information, especially when dealing with significant blur, which can lead to inaccurate final generated structures. To address this challenge, we propose a method that incorporates an LKPN trained simultaneously with the diffusion model. The LKPN dynamically estimates pixel-specific deblurring kernels at each step of the diffusion process. These kernels are adaptively adjusted based on local content by the element-wise adaptive convolution(EAC), enabling the model to address spatially varying blur patterns effectively in the latent space. By leveraging intermediate image priors generated during the diffusion process, the EAC can generate clear structural guidance, which is then used as conditional inputs to the diffusion model. This iterative refinement allows the LKPN to progressively improve the accuracy of deblurred results by EAC, leading to increasingly clearer intermediate results while preserving the information of the input image.

Specifically, we first employ a pre-trained and frozen VAE encoder initialized from SD to encode the blurry image and the clear one into the latent space, obtaining their corresponding latent representations z_{lq} and z_0 . We follow the Eq.(1) to add noise to z_0 , obtaining z_t . Then the LKPN, which is a U-Net architecture, predicts a spatially variant kernel in latent space at step t :

$$k_t = \text{LKPN}(z_t, z_{lq}, t), \quad (3)$$

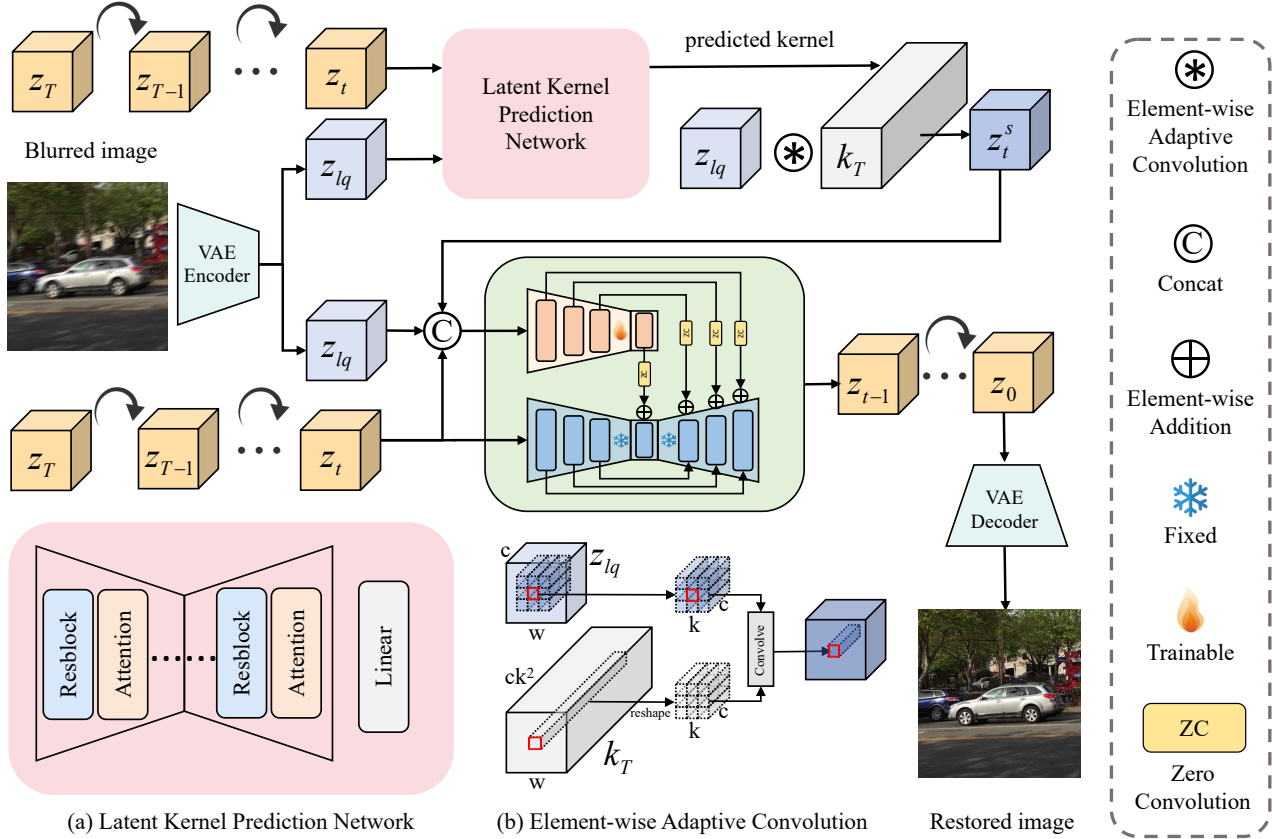


Figure 3. Overall architecture of the proposed DeblurDiff. It integrates a Latent Kernel Prediction Network (LKPN) with a generative diffusion model to address the challenges of real-world image deblurring. The LKPN progressively recovers clear structures from blurred images by estimating pixel-specific deblurring kernels at each step of the diffusion process. These kernels are adaptively adjusted based on local content and applied through Element-wise Adaptive Convolution (EAC). The refined clear z^s is used as a condition to guide the diffusion process, enabling the model to effectively preserve the input information and structural integrity.

where k_t is the predicted kernel at time step t . Then k_t is used to refine the blurry image in the latent space by :

$$z_t^s = \text{EAC}(z_{lq}, k_t), \quad (4)$$

where EAC is the element-wise adaptive convolution in Figure 3(b) and z_t^s is the deblurred latent. In the appendix, we provide a detailed explanation of the LKPN and EAC architecture.

During training, the LKPN is trained simultaneously with the diffusion model. The LKPN follows the framework of DDPM, imposing constraints simultaneously in both the latent space and the pixel space to progressively optimize the kernel estimation. Specifically, our objective is to minimize the following objective:

$$\begin{aligned} \mathcal{L}_{\text{LKPN}} &= \mathcal{L}_{\text{latent}} + \mathcal{L}_{\text{pixel}}, \\ \mathcal{L}_{\text{latent}} &= \mathbb{E}_{z_0, z_{lq}, k_t} \left[\|z_0 - \text{EAC}(z_{lq}, k_t)\|_2^2 \right], \\ \mathcal{L}_{\text{pixel}} &= \mathbb{E}_{z_0, z_{lq}, k_t} \left[\|\mathcal{D}(z_0) - \mathcal{D}(\text{C}(z_{lq}, k_t))\|_2^2 \right], \end{aligned} \quad (5)$$

where EAC denotes the element-wise adaptive convolution

(EAC) in Figure 3(b), and \mathcal{D} denotes the pre-trained VAE decoder of SD. The network architecture of the proposed LKPN is shown in Figure 3.

3.3. Conditional diffusion for image deblurring .

For the conditional generation network, we follow the training methodology of ControlNet (Zhang et al., 2023), given its demonstrated effectiveness in conditional image generation. Specifically, we adopt the encoder of the UNet in SD as a trainable conditional control branch and initialize the control network by copying weights from the pre-trained SD model. We concatenate z^s recovered by the EAC and z_{lq} as the input to the ControlNet, which is initialized with the weights of SD. We provide a detailed explanation of the network architecture in the appendix. During training, the LKPN and ControlNet are jointly trained following the framework of DDPM (Ho et al., 2020), we minimize the following loss function:

$$\mathcal{L} = \mathcal{L}_{\text{denoise}} + \mathcal{L}_{\text{LKPN}}. \quad (6)$$

DeblurDiff: Real-World Image Deblurring with Generative Diffusion Models

Table 1. Quantitative evaluations of the proposed method against state-of-the-art ones on both synthetic and real-world benchmarks. The models marked with an asterisk * indicate that we retrain them on our own training set. The best and second performances are marked in red and blue, respectively. For the RWBI and Real Blurry Images datasets, which lack ground truth (GT) data, we evaluate the performance using only no-reference metrics.

Dataset	Metrics	FFTformer*	DBGAN	ResShift	HI-Diff	ControlNet*	PASD*	DiffBIR*	Ours
GoPro	PSNR \uparrow	26.86	31.18	29.03	33.33	22.31	22.82	23.86	24.32
	SSIM \uparrow	0.8357	0.9182	0.8781	0.9462	0.6547	0.6559	0.7173	0.7375
	LPIPS \downarrow	0.1538	0.1120	0.0780	0.0820	0.3292	0.2984	0.2772	0.2191
	NIQE \downarrow	4.1200	5.1988	4.8367	4.6119	3.5305	2.6567	3.4193	3.1769
	MUSIQ \uparrow	52.2993	42.0985	44.2820	47.7791	59.4246	61.5345	56.3249	61.6369
	MANIQA \uparrow	0.5454	0.4976	0.9419	0.6119	0.5746	0.5904	0.5464	0.6134
	CLIP-IQA \uparrow	0.4360	0.3788	0.4229	0.4841	0.5869	0.5758	0.5260	0.5966
DVD	PSNR \uparrow	27.07	27.78	27.78	30.31	22.03	22.23	23.49	23.74
	SSIM \uparrow	0.8534	0.8356	0.8420	0.8972	0.6409	0.6440	0.7114	0.7055
	LPIPS \downarrow	0.1628	0.2126	0.1249	0.1363	0.3330	0.2968	0.2795	0.2501
	NIQE \downarrow	3.8562	4.8188	4.6422	5.1858	3.4037	3.2504	3.1357	2.7822
	MUSIQ \uparrow	60.1091	40.4781	52.7551	45.5395	65.3657	68.3299	61.6415	67.2447
	MANIQA \uparrow	0.6257	0.5548	0.5744	0.5360	0.6155	0.6409	0.5773	0.6480
	CLIP-IQA \uparrow	0.5271	0.4346	0.4831	0.4065	0.6606	0.6528	0.5829	0.6686
Realblur	PSNR \uparrow	26.94	23.91	26.30	30.18	23.77	25.02	25.50	25.71
	SSIM \uparrow	0.8580	0.7434	0.8140	0.9049	0.6787	0.7642	0.7724	0.7705
	LPIPS \downarrow	0.1411	0.2945	0.1249	0.0868	0.2565	0.2075	0.1951	0.1693
	NIQE \downarrow	4.3473	5.3228	5.2628	5.1437	4.6525	3.9192	4.3053	4.2666
	MUSIQ \uparrow	61.5808	38.4866	49.3209	57.1640	66.5174	61.1498	58.7450	65.0557
	MANIQA \uparrow	0.6374	0.43222	0.5373	0.6218	0.6452	0.5994	0.5869	0.6538
	CLIP-IQA \uparrow	0.5336	0.3469	0.4521	0.5101	0.6041	0.5457	0.5261	0.6087
RWBI	NIQE \downarrow	4.4631	5.2905	5.4446	5.3373	5.0331	4.1973	4.2742	4.5171
	MUSIQ \uparrow	59.6223	42.7631	51.0359	47.1820	62.5079	62.1680	61.8865	66.7505
	MANIQA \uparrow	0.5425	0.4852	0.4953	0.5082	0.5758	0.5645	0.5618	0.6260
	CLIP-IQA \uparrow	0.5413	0.3645	0.5032	0.3907	0.6199	0.5820	0.6042	0.6849
Real Images	NIQE \downarrow	3.8520	4.9338	5.4704	4.7018	4.0978	4.4460	3.7964	3.6628
	MUSIQ \uparrow	52.9290	32.0568	48.8154	43.8702	51.5191	61.6320	53.6088	52.9263
	MANIQA \uparrow	0.5170	0.4488	0.5345	0.5722	0.5544	0.5937	0.5564	0.5963
	CLIP-IQA \uparrow	0.5026	0.3501	0.4767	0.4545	0.5254	0.5919	0.5384	0.5496

3.4. Sampling process of the DeblurDiff.

During the inference stage, the LKPN first estimates the initial spatially variant kernel from random Gaussian noise and the blurred image, which is used to obtain an initial conditional z_T^s . The controlled diffusion model uses z_T^s and z_{lq} as conditions to generate an initial clear result z_{T-1} . Subsequently, z_{T-1} is fed back into the LKPN to help estimate a more accurate kernel:

$$k_{T-1} = \text{LKPN}(z_{T-1}, z_{lq}, T-1), \quad (7)$$

thereby iteratively optimizing the generated results in subsequent steps. Please see the appendix for more details.

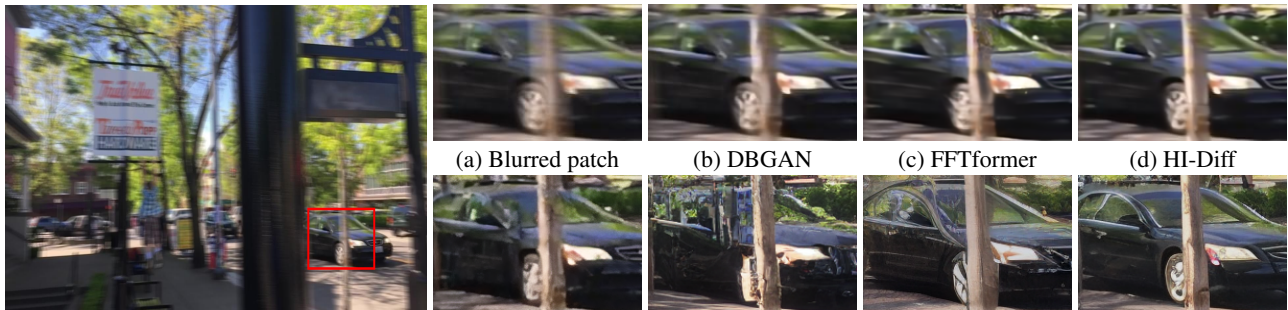
This synergy between the LKPN and the diffusion model creates a mutually reinforcing cycle, where clear structural guidance from the LKPN improves the diffusion process, and intermediate results from the diffusion model further refine the deblurred results.

4. Experimental Results

4.1. Experimental Settings

Training Datasets. Current existing deblurring datasets are generally small in scale and low in resolution, which are insufficient for effectively training diffusion models. Therefore, we do not use common deblurring datasets such as GoPro (Nah et al., 2017) as our training set. Instead We have collected and created a large-scale dataset containing approximately 500,000 data pairs. Our training dataset consists of three parts: (1) Existing deblurring datasets (including MC-Blur (Zhang et al., 2024) and RSBlur (Rim et al., 2022)). (2) We collect and capture some high-definition video clips, generating blurred and clear data pairs using the same strategy as REDS (Nah et al., 2019). (3) We collect a large number of high-definition images and generate various motion blur kernels to synthesize corresponding blurred images. We provide more details about the training dataset in the appendix.

Test Datasets. We evaluate the proposed DeblurDiff on commonly used image deblurring dataset, including synthetic datasets (GoPro (Nah et al., 2017), DVD (Su et al.,



Blurred image from DVD dataset

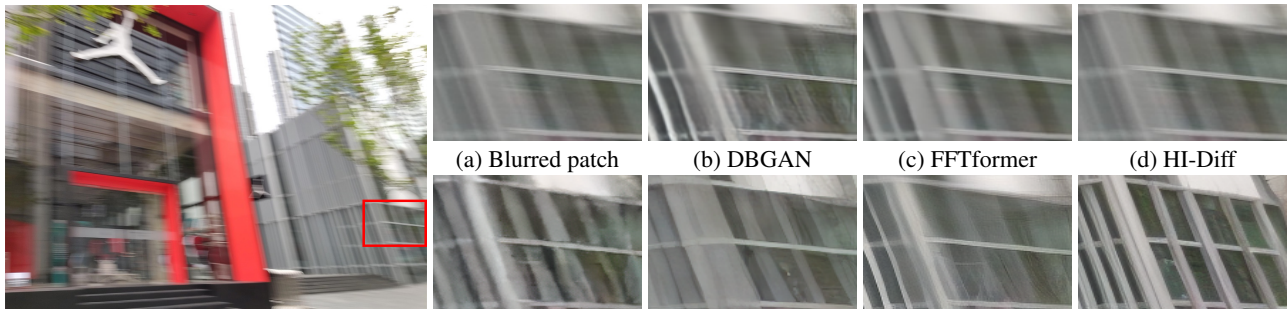
(e) ResShift

(f) PASD

(g) DiffBIR

(h) Ours

Figure 4. Deblurred results on the DVD dataset (Su et al., 2017). Existing methods struggle to effectively restore clear images. In contrast, our approach not only removes blur but also recovers sharp structures and fine details.



Blurred image from RWBI dataset

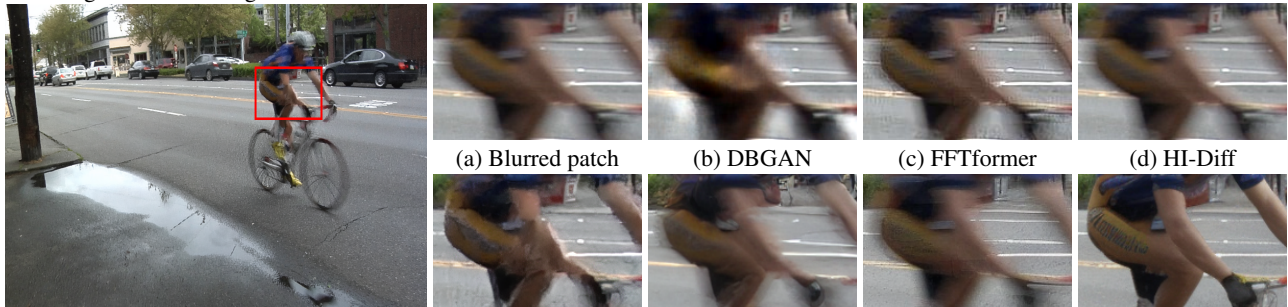
(e) ResShift

(f) PASD

(g) DiffBIR

(h) Ours

Figure 5. Deblurred results on the RWBI dataset (Zhang et al., 2020). The structures are not recovered well in (b)-(g). The proposed method generates an image with much clearer structures.



Blurred image from Real Blurry Images

(e) ResShift

(f) PASD

(g) DiffBIR

(h) Ours

Figure 6. Deblurred results on real blurry images dataset (Cho et al., 2012). The deblurred results in (b)-(g) still contain significant blur effects. The proposed method generates a clear image.

2017)) and Real Blurry Images (Cho et al., 2012), Real-Blur (Rim et al., 2020), RWBI (Zhang et al., 2020).

Implementation Details. We employ the Adam optimizer (Kingma & Ba, 2015) to train DeblurDiff with a batch size of 128. The learning rate is set to a fixed value of 5×10^{-5} . The model is trained for 100K iterations using 8 NVIDIA 80G-A100 GPUs, each with 80GB of memory.

Evaluation Metrics. We employ a range of reference-based and no-reference metrics to provide a comprehensive evaluation of the deblurring performance. For fidelity and perceptual quality assessment, we employ reference-based metrics, including PSNR, SSIM, and LPIPS (Zhang et al., 2018). For no-reference evaluation, we include NIQE (Zhang et al., 2015), MANIQA (Yang et al., 2022), MUSIQ (Ke et al., 2021), and CLIPIQA (Wang et al., 2023), which assess

image quality based on statistical and learning-based approaches. This diverse set of metrics ensures a thorough analysis of both fidelity and perceptual quality.

Compared Methods. We compare our DeblurDiff with several state-of-the-art image deblurring methods, which are categorized into two groups: (1) non-diffusion-based methods, including FFTformer (a transformer-based regression approach) (Kong et al., 2023) and DBGAN (a GAN-based method) (Zhang et al., 2020), and (2) diffusion-based methods, including HiDiff (Chen et al., 2023), ResShift (Yue et al., 2024), ControlNet (Zhang et al., 2023), PASD (Yang et al., 2024), and DiffBIR (Lin et al., 2025). To ensure a fair comparison, we retrain FFTformer on our training dataset. We employ the pre-trained FFTformer as the Degradation Removal Module (DRM) in DiffBIR and retrain DiffBIR, as the original DiffBIR framework is not designed for de-

Table 2. Effectiveness of each component in the proposed method on the real blurry images (Cho et al., 2012).

	LKPN	EAC	SD prior for LKPN	NIQE	MANIQA
ControlNet	✗	✗	✗	4.0978	0.5544
w/o EAC	✓	✗	✓	4.0230	0.5874
w/o SD for LKPN	✓	✓	✗	3.8087	0.5882
DeblurDiff	✓	✓	✓	3.6628	0.5963

blurring tasks. We also train a ControlNet and PASD for image deblurring tasks. All the aforementioned pretrained methods are trained and tested using the publicly released codes and models of the competing methods, ensuring a fair and consistent comparison under the same dataset and training settings as our proposed method.

4.2. Comparisons with the state of the arts

We evaluate our approach on the synthetic and real-world datasets. Table 1 shows the quantitative results. Our method shows strong performance in no-reference metrics, achieving higher scores compared to existing approaches. This indicates that our method excels in perceptual quality and realism, which are critical for real-world applications where ground truth images are often unavailable. Our method achieves lower scores in reference-based metrics compared to HI-Diff. However, HI-Diff does not utilize a pre-trained SD model, thus focusing more on reference-based metrics while lacking generative capabilities, which results in relatively worse performance in no-reference metrics.

Figure 4 shows visual comparisons on the synthetic dataset of DVD (Su et al., 2017). The GAN-based method (Zhang et al., 2020) exhibits significantly inferior deblurring performance, failing to restore clear structures and fine details effectively. Existing diffusion-based methods, such as HiDiff (Chen et al., 2023) and ResShift (Yue et al., 2024), fail to achieve satisfactory results in Figure 4 (d) and (e) due to their lack of SD priors, which leads to suboptimal generation quality in terms of both structural clarity and detail fidelity. Leveraging the pre-trained FFTformer (Kong et al., 2023) to preprocess blurred images Figure 4 (c) and subsequently applying diffusion-based restoration can partially remove blur. However, since FFTformer sometimes cannot eliminate blur and tends to introduce undesirable artifacts during preprocessing, the final results generated by DiffBIR often exhibit unnatural structures and are inconsistent with the input. In contrast, our method, guided by the LKPN that progressively generates clear structures, produces better results with sharper and more accurate structures.

Figure 5 and Figure 6 present the visual comparison results on the real-world dataset. DBGAN (Zhang et al., 2020) and FFTformer (Kong et al., 2023) struggle to recover clear structures from severe blur, while Hi-Diff (Chen et al., 2023) and ResShift (Yue et al., 2024) fail to reconstruct fine details due to the lack of pre-trained image priors. PASD (Yang et al., 2024) and DiffBIR (Lin et al., 2025), which rely on degradation removal models for pre-deblurring, often produce suboptimal results with noticeable artifacts, as these

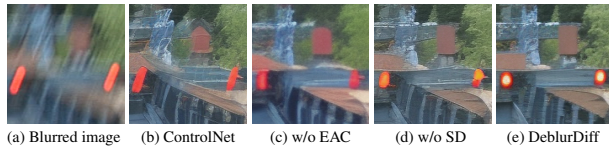


Figure 7. Effectiveness of the proposed DeblurDiff on image deblurring. We provide more detailed results in the appendix.

models cannot effectively handle complex blur patterns. In contrast, our method demonstrates better performance in both structural recovery and detail reconstruction. The LKPN progressively generates clear structures and adaptively refines the deblurring process, enabling our approach to achieve high-quality results with minimal artifacts.

4.3. Analysis experiments.

The proposed LKPN is used to leverage intermediate clear priors generated during the diffusion process, providing clear structural guidance as conditional inputs to the diffusion model. When the blurry image is directly used as the conditional input (ControlNet for short), the diffusion model struggles to recover clear structures and fine details (Figure 7(b)), particularly in cases of severe blur. This is because the blurry image lacks sufficient structural information to guide the generation process effectively, leading to suboptimal deblurring performance. Table 2 shows the quantitative evaluation results on the real blurry images dataset. When the LKPN is modified to directly predict the deblurred result in the latent space to serve as the conditional input for diffusion, instead of estimating element-wise adaptive kernels (w/o EAC for short), the performance is worse compared to our proposed method that predicts a kernel and uses EAC to generate a clear guidance. This approach fails to adaptively address distinct blur characteristics at each pixel location, resulting in artifacts and inconsistencies in the generated images. Additionally, it cannot effectively preserve the input information and structural integrity, leading to a loss of important details and coherence in the deblurred results (Figure 7(c)). In contrast, our full method, which estimates pixel-specific deblurring kernels, dynamically adjusts to local content, enabling more accurate deblurring.

To further validate the effectiveness of leveraging clear priors from the diffusion process in the LKPN, we compare our method with the baseline that directly estimates the kernel from the blurry image without utilizing the intermediate results from the diffusion process (w/o SD for LKPN for short). In this baseline, the estimated kernel is applied to the blurry image to generate a deblurred result, which is then used as a conditional input to the diffusion model. However, this approach lacks the iterative refinement provided by intermediate image priors from the diffusion process. As a result, the LKPN struggles to provide accurate structural guidance, leading to structural errors and inconsistencies in the generated results, as shown in Figure 7(d).

5. Conclusion

In this paper, we propose DeblurDiff, a framework for real-world image deblurring that integrates a Latent Kernel Prediction Network (LKPN) with a generative diffusion model. Our approach addresses the limitations of existing methods by leveraging the priors of pre-trained SD models and introducing an adaptive mechanism to estimate pixel-specific kernels. These kernels are applied through Element-wise Adaptive Convolution (EAC), which adaptively adjusts to local content, enabling the model to preserve input information and structural integrity effectively. Through extensive experiments on both synthetic and real-world benchmarks, we demonstrated that DeblurDiff performs favorably against state-of-the-art methods in terms of structural fidelity and visual quality.

References

- Boracchi, G. and Foi, A. Modeling the performance of image restoration from motion blur. *Image Processing, IEEE Transactions on*, 21(8):3502–3517, aug. 2012.
- Chen, L., Chu, X., Zhang, X., and Sun, J. Simple baselines for image restoration. In *ECCV*, 2022.
- Chen, Z., Zhang, Y., Ding, L., Bin, X., Gu, J., Kong, L., and Yuan, X. Hierarchical integration diffusion model for realistic image deblurring. In *NeurIPS*, 2023.
- Cho, S., Wang, J., and Lee, S. Video deblurring for hand-held cameras using patch-based synthesis. *ACM Transactions on Graphics (TOG)*, 31:1–9, 2012.
- Cho, S.-J., Ji, S.-W., Hong, J.-P., Jung, S.-W., and Ko, S.-J. Rethinking coarse-to-fine approach in single image deblurring. In *ICCV*, 2021.
- Dhariwal, P. and Nichol, A. Diffusion models beat gans on image synthesis. In *NeurIPS*, 2021.
- He, K., Zhang, X., Ren, S., and Sun, J. Deep residual learning for image recognition. In *CVPR*, 2016.
- Ho, J., Jain, A., and Abbeel, P. Denoising diffusion probabilistic models. In *NeurIPS*, 2020.
- Ke, J., Wang, Q., Wang, Y., Milanfar, P., and Yang, F. Musiq: Multi-scale image quality transformer. In *ICCV*, 2021.
- Kingma, D. P. and Ba, J. Adam: A method for stochastic optimization. In *ICLR*, 2015.
- Kong, L., Dong, J., Ge, J., Li, M., and Pan, J. Efficient frequency domain-based transformers for high-quality image deblurring. In *CVPR*, 2023.
- Krishnan, D., Tay, T., and Fergus, R. Blind deconvolution using a normalized sparsity measure. In *CVPR*, 2011.
- Kupyn, O., Budzan, V., Mykhailych, M., Mishkin, D., and Matas, J. Deblurgan: Blind motion deblurring using conditional adversarial networks. In *CVPR*, 2018.
- Kupyn, O., Martyniuk, T., Wu, J., and Wang, Z. Deblurgan-v2: Deblurring (orders-of-magnitude) faster and better. In *ICCV*, 2019.
- Ledig, C., Theis, L., Huszár, F., Caballero, J., Cunningham, A., Acosta, A., Aitken, A., Tejani, A., Totz, J., Wang, Z., et al. Photo-realistic single image super-resolution using a generative adversarial network. In *CVPR*, 2017.
- Li, Y., Fan, Y., Xiang, X., Demandolx, D., Ranjan, R., Timofte, R., and Van Gool, L. Efficient and explicit modelling of image hierarchies for image restoration. In *CVPR*, 2023.
- Lin, X., He, J., Chen, Z., Lyu, Z., Dai, B., Yu, F., Qiao, Y., Ouyang, W., and Dong, C. Diffbir: Toward blind image restoration with generative diffusion prior. In *ECCV*, 2025.
- Lugmayr, A., Danelljan, M., Van Gool, L., and Timofte, R. Srfflow: Learning the super-resolution space with normalizing flow. In *ECCV*, 2020.
- Nah, S., Kim, T. H., and Lee, K. M. Deep multi-scale convolutional neural network for dynamic scene deblurring. In *CVPR*, 2017.
- Nah, S., Baik, S., Hong, S., Moon, G., Son, S., Timofte, R., and Mu Lee, K. Ntire 2019 challenge on video deblurring and super-resolution: Dataset and study. In *CVPRW*, 2019.
- Pan, J., Sun, D., Pfister, H., and Yang, M.-H. Blind image deblurring using dark channel prior. In *CVPR*, 2016.
- Pan, J., Hu, Z., Su, Z., and Yang, M.-H. l_0 -regularized intensity and gradient prior for deblurring text images and beyond. *IEEE Transactions on Pattern Analysis and Machine Intelligence*, 39(2):342–355, 2017. doi: 10.1109/TPAMI.2016.2551244.
- Pan, J., Dong, J., Liu, Y., Zhang, J., Ren, J. S. J., Tang, J., Tai, Y.-W., and Yang, M.-H. Physics-based generative adversarial models for image restoration and beyond. *IEEE TPAMI*, 43(7):2449–2462, 2021.
- Ravi, N., Gabeur, V., Hu, Y.-T., Hu, R., Ryali, C., Ma, T., Khedr, H., Rädle, R., Rolland, C., Gustafson, L., Mintun, E., Pan, J., Alwala, K. V., Carion, N., Wu, C.-Y., Girshick, R., Dollár, P., and Feichtenhofer, C. Sam 2: Segment anything in images and videos. *arXiv preprint arXiv:2408.00714*, 2024.

- Ren, M., Delbracio, M., Talebi, H., Gerig, G., and Milanfar, P. Multiscale structure guided diffusion for image deblurring. In *CVPR*, 2023.
- Rim, J., Lee, H., Won, J., and Cho, S. Real-world blur dataset for learning and benchmarking deblurring algorithms. In *ECCV*, 2020.
- Rim, J., Kim, G., Kim, J., Lee, J., Lee, S., and Cho, S. Realistic blur synthesis for learning image deblurring. In *ECCV*, 2022.
- Rombach, R., Blattmann, A., Lorenz, D., Esser, P., and Ommer, B. High-resolution image synthesis with latent diffusion models. In *CVPR*, 2022.
- Su, S., Delbracio, M., Wang, J., Sapiro, G., Heidrich, W., and Wang, O. Deep video deblurring for hand-held cameras. In *CVPR*, 2017.
- Tao, X., Gao, H., Shen, X., Wang, J., and Jia, J. Scale-recurrent network for deep image deblurring. In *CVPR*, 2018.
- Vaswani, A., Shazeer, N., Parmar, N., Uszkoreit, J., Jones, L., Gomez, A. N., Kaiser, L., and Polosukhin, I. Attention is all you need. In *NIPS*, 2017.
- Wang, J., Chan, K. C., and Loy, C. C. Exploring clip for assessing the look and feel of images. In *AAAI*, 2023.
- Wang, Z., Cun, X., Bao, J., Zhou, W., Liu, J., and Li, H. Uformer: A general u-shaped transformer for image restoration. In *CVPR*, 2022.
- Yang, S., Wu, T., Shi, S., Lao, S., Gong, Y., Cao, M., Wang, J., and Yang, Y. Maniqa: Multi-dimension attention network for no-reference image quality assessment. In *CVPR*, 2022.
- Yang, T., Wu, R., Ren, P., Xie, X., and Zhang, L. Pixel-aware stable diffusion for realistic image super-resolution and personalized stylization. In *ECCV*, 2024.
- Yuan, L., Sun, J., Quan, L., and Shum, H.-Y. Image deblurring with blurred/noisy image pairs. *ACM Trans. Graph.*, 26(3), 2007.
- Yue, Z., Wang, J., and Loy, C. C. Resshift: Efficient diffusion model for image super-resolution by residual shifting. In *NeurIPS*, 2024.
- Zamir, S. W., Arora, A., Khan, S., Hayat, M., Khan, F. S., Yang, M.-H., and Shao, L. Multi-stage progressive image restoration. In *CVPR*, 2021.
- Zamir, S. W., Arora, A., Khan, S., Hayat, M., Khan, F. S., and Yang, M.-H. Restormer: Efficient transformer for high-resolution image restoration. In *CVPR*, 2022.
- Zhang, K., Luo, W., Zhong, Y., Ma, L., Stenger, B., Liu, W., and Li, H. Deblurring by realistic blurring. In *CVPR*, 2020.
- Zhang, K., Wang, T., Luo, W., Ren, W., Stenger, B., Liu, W., Li, H., and Yang, M.-H. Mc-blur: A comprehensive benchmark for image deblurring. *IEEE Transactions on Circuits and Systems for Video Technology*, 34(5):3755–3767, 2024.
- Zhang, L., Zhang, L., and Bovik, A. C. A feature-enriched completely blind image quality evaluator. *IEEE Transactions on Image Processing*, 24(8):2579–2591, 2015.
- Zhang, L., Rao, A., and Agrawala, M. Adding conditional control to text-to-image diffusion models. In *ICCV*, 2023.
- Zhang, R., Isola, P., Efros, A. A., Shechtman, E., and Wang, O. The unreasonable effectiveness of deep features as a perceptual metric. In *CVPR*, 2018.
- Zhao, Y., Po, L.-M., Ye, X., Xu, Y., and Yan, Q. Modeling dual-exposure quad-bayer patterns for joint denoising and deblurring. *IEEE Transactions on Image Processing*, 2024.
- Zhou, S., Zhang, J., Pan, J., Xie, H., Zuo, W., and Ren, J. Spatio-temporal filter adaptive network for video deblurring. In *ICCV*, 2019.

A. Training datasets.

As mentioned in the main paper, existing deblurring datasets such as GoPro (Nah et al., 2017) and DVD (Su et al., 2017) have several limitations. These datasets typically contain a relatively small number of images (usually only a few thousand) and a limited variety of scenes (often only a few dozen). This insufficiency makes it difficult to train a robust deblurring diffusion model. Moreover, for the GoPro dataset, which uses multi-frame video sequences to synthesize blur, the low frame rate of the videos results in blur patterns that significantly differ from real-world blur. Therefore, we do not train our model on these problematic datasets. Instead, we constructed a large-scale dataset to train our DeblurDiff model. This dataset addresses the limitations of existing datasets by providing a richer and more diverse set of image pairs, thereby better supporting the learning and generalization capabilities of the model.

Our training dataset consists of three parts: (1) Existing deblurring datasets, including MC-Blur (Zhang et al., 2024) and RSBlur (Rim et al., 2022), which contain high-resolution blur-sharp data pairs (approximately 100,000 images). Some of their training data pairs are illustrated in Figure 8. (2) We capture some high-frame-rate high-definition video clips, generating blurred and clear data pairs (approximately 200,000 images) using the same strategy as REDS (Nah et al., 2019). We present some of our clear and blurred data pairs in Figure 9. (3) We collected a large number of high-definition images as ground truth (approximately 200,000 images) and generated various motion blur kernels to synthesize corresponding blurred images. Specifically, using the method proposed by (Boracchi & Foi, 2012), we generated 100,000 motion blur kernels (some of which are presented in Figure 10). The size of the motion kernel is 63×63 , and we randomly generate motion trajectories within this range, with the length of the trajectory being a random number between 1 and 1000. We use these kernels and high-definition images to synthesize two types of blurred and clear data pairs: globally uniform blur and non-uniform blur. For globally uniform blur, we directly use the generated kernel as the blur kernel to convolve with the clear image, obtaining the corresponding blurred image. For non-uniform blur, we use the SAM2 (Ravi et al., 2024) to segment objects in the sharp image and apply different motion blur kernels to different objects to simulate the inconsistent blur caused by the motion of different objects in the real world. We present the training data pairs for globally uniform blur and non-uniform blur in Figures 11 and Figure 12, respectively.

B. Comparison with More Methods.

For a fair comparison, we provide a comparison of the results using the official FFTformer training weights on the

Table 3. Quantitative evaluations of the original FFTformer and the FFTformer* we retrained on both synthetic and real-world benchmarks. The models marked with an asterisk * indicate that we retrain them on our own training set. The best is marked in red. For the RWBI and Real Blurry Images datasets, which lack ground truth (GT) data, we evaluate the performance using only no-reference metrics.

Dataset	Metrics	FFTformer	FFTformer*
GoPro	PSNR \uparrow	34.21	26.86
	SSIM \uparrow	0.9536	0.8357
	LPIPS \downarrow	0.0725	0.1538
	NIQE \downarrow	5.0338	4.1200
	MUSIQ \uparrow	46.0739	52.2993
	MANIQA \uparrow	0.5442	0.5454
	CLIP-IQA \uparrow	0.4139	0.4360
DVD	PSNR \uparrow	27.29	27.07
	SSIM \uparrow	0.8426	0.8534
	LPIPS \downarrow	0.1993	0.1628
	NIQE \downarrow	4.7344	3.8562
	MUSIQ \uparrow	40.0924	60.1091
	MANIQA \uparrow	0.5653	0.6257
	CLIP-IQA \uparrow	0.4454	0.5271
Realblur	PSNR \uparrow	29.97	26.94
	SSIM \uparrow	0.9036	0.8580
	LPIPS \downarrow	0.0906	0.1411
	NIQE \downarrow	5.1833	4.3473
	MUSIQ \uparrow	52.2186	61.5808
	MANIQA \uparrow	0.6151	0.6374
	CLIP-IQA \uparrow	0.5077	0.5336
RWBI	NIQE \downarrow	4.9704	4.4631
	MUSIQ \uparrow	43.0404	59.6223
	MANIQA \uparrow	0.5201	0.5425
	CLIP-IQA \uparrow	0.3749	0.5413
Real Images	NIQE \downarrow	4.4877	3.8520
	MUSIQ \uparrow	38.1174	52.9290
	MANIQA \uparrow	0.5487	0.5170
	CLIP-IQA \uparrow	0.4222	0.5026

test dataset and the results after retraining on our own training dataset, as shown in Table 3. Apart from the significant difference on the GoPro dataset, which is expected since the FFTformer was trained on the GoPro training set while our training dataset does not include GoPro data, our retrained method achieves comparable performance to the original FFTformer on most metrics across other datasets.



Figure 8. Blurred and clear training data pairs in the RSBlur dataset (Rim et al., 2022).



Figure 9. Blurred and clear training data pairs synthesized using consecutive video frames.

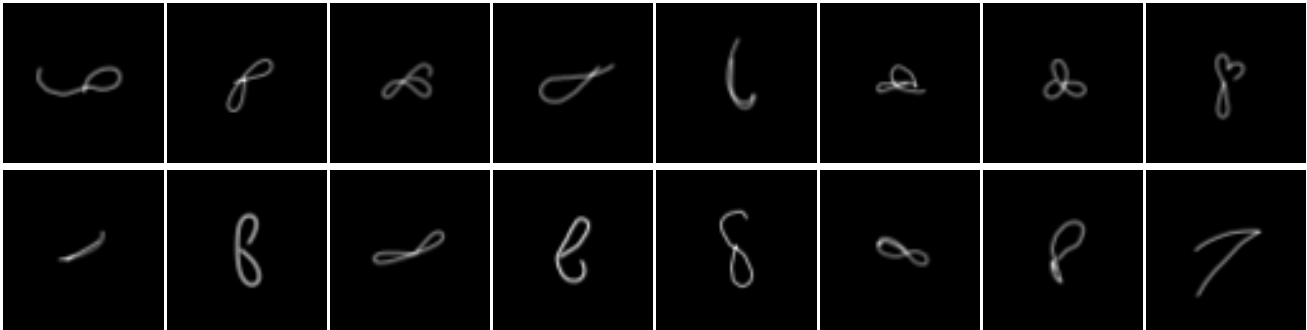


Figure 10. Motion blur kernels generated by (Boracchi & Foi, 2012).



Figure 11. Training data pairs of globally uniform blurred images and clear images.



Figure 12. Training data pairs of globally non-uniform blurred images and clear images.

C. The specific architecture of the DeblurDiff.

LKPN is a UNet structure with 4 layers of encoders and decoders, each layer comprising two blocks, which consist of a ResBlock (He et al., 2016) and a self-attention (Vaswani et al., 2017) layer as shown in Figure 3. The input to the LKPN is formed by concatenating z_t and z_{lq} . Additionally, the time step t is embedded into the same dimension using a linear layer and added before the out_layer of the ResBlock. Given an input z_{lq} with a shape of (c, h, w) after encoding with the VAE encoder. After passing through the LKPN’s UNet, the shape of the output features remains (c, h, w) . At the end of the LKPN, a linear layer is used to transform the shape into $(c \times k \times k, h, w)$, where k represents the size of the spatially variant kernel we estimate. In this paper, we use $k = 5$.

EAC is used to restore the latent of the clear image while preserving the input information by utilizing the spatially-variant kernel estimated by the LKPN. The EAC first reshapes the kernel estimated by the LKPN into (h, w, ck^2) . For each position (h_i, w_i, c_i) of $z_{lq} \in \mathbb{R}^{h \times w}$, a spatially kernel $\mathcal{F}_{h_i, w_i, c_i} \in \mathbb{R}^{k \times k}$ is applied to the region centered around $z_{lq}(h_i, w_i, c_i)$ as follows:

$$\begin{aligned} \hat{z}_{lq}(h_i, w_i, c_i) &= \mathcal{F}_{h_i, w_i, c_i} * z_{lq}(h_i, w_i, c_i) \\ &= \sum_{n=-r}^r \sum_{m=-r}^r \mathcal{F}(h_i, w_i, k^2 c_i + kn + m) \\ &\quad \times z_{lq}(h_i - n, w_i - m, c_i), \end{aligned} \quad (8)$$

where $r = \frac{k-1}{2}$, $*$ denotes convolution operation, \mathcal{F} is the generated filter, $z_{lq}(h_i - n, w_i - m, c_i)$ and $\hat{z}_{lq}(h_i, w_i, c_i)$ denote the input features and transformed features, respectively.

ControlNet is used to enhance the capabilities of pre-trained SD models by introducing additional conditional inputs to precisely control the image generation process as shown in Figure 3. Specifically, ControlNet guides the diffusion process by integrating a conditioning input (e.g., a blurry

Algorithm 1 DeblurDiff Sampling

Input: Blurry image X_B
Output: Deblurred image X_D
 $z_{lq} = \mathcal{E}(X_B)$
 $z_T \sim \mathcal{N}(0, I)$
for $t = T, \dots, 1$ **do**
 $z \sim \mathcal{N}(0, I)$ if $t > 1$, else $z = 0$
 $k_t = \text{LKPN}(z_t, z_{lq}, t)$
 $z_t^s = \text{EAC}(z_{lq}, k_t)$
 $\epsilon_{pred, t} = \text{ControlNet}(z_t^s, z_{lq}, z_t, t)$
 $z_{t-1} = \frac{1}{\sqrt{\alpha_t}} \left(z_t - \frac{1-\alpha_t}{\sqrt{1-\alpha_t}} \epsilon_{pred, t} \right) + \sigma_t z$
end for

image) with the noisy latent representation from the diffusion model. Initialized with pre-trained diffusion model weights, ControlNet uses ZeroConv layers (1x1 convolutions initialized with zero weights) to gradually incorporate the conditioning input without disrupting the pre-trained knowledge. This allows the model to iteratively refine the latent representation, generating high-quality outputs that align with the provided guidance. We use the concatenated z_{lq} and z^s obtained from EAC as conditional inputs. For the first layer, we do not use the weights from the original SD model for initialization, since our input channels differ from those of the original SD. Instead, we used random initialization.

The sampling process of DeblurDiff is shown in Algorithm 1.

D. Visual comparison of the ablation study.

We provide the specific structural diagrams of the corresponding baselines in the ablation study in Figures Figures 15 to 17.

When the LKPN does not utilize the intermediate clear priors from the diffusion process (referred to as w/o SD for LKPN) 17, it estimates the deblurring result directly from the blurry image in the latent space throughout the entire iterative process.

Since the LKPN lacks the guidance of intermediate clear priors, its predictions remain static and do not improve over time (Figure 13(a)). As a result, the deblurred results at each step are identical, leading to suboptimal performance and the inability to recover sharp structures or fine details effectively (Figure 14(d)).

When the LKPN directly predicts the deblurred result in the latent space 16 instead of estimating a spatially variant kernel and applying it through the EAC (referred to as w/o EAC), the generated results tend to be overly smooth (Figure 13(b)). This approach fails to adaptively address distinct blur characteristics at each pixel location, resulting in the loss of important structural details and the inability to effectively preserve the input information. As a consequence, the deblurred images lack sharpness and fine details, leading to suboptimal visual quality (Figure 14(c)).

In contrast, our method leverages intermediate clear priors from the diffusion process to iteratively refine the spatially variant kernels estimated by the LKPN. This iterative refinement enables the LKPN to progressively improve its predictions, generating increasingly accurate deblurring results (Figure 13(c)). The refined kernels are then applied through the Element-wise Adaptive Convolution (EAC), which adaptively addresses distinct blur characteristics at each pixel location, effectively preserving the input information and recovering sharp structures and fine details (Figure 14(e)).

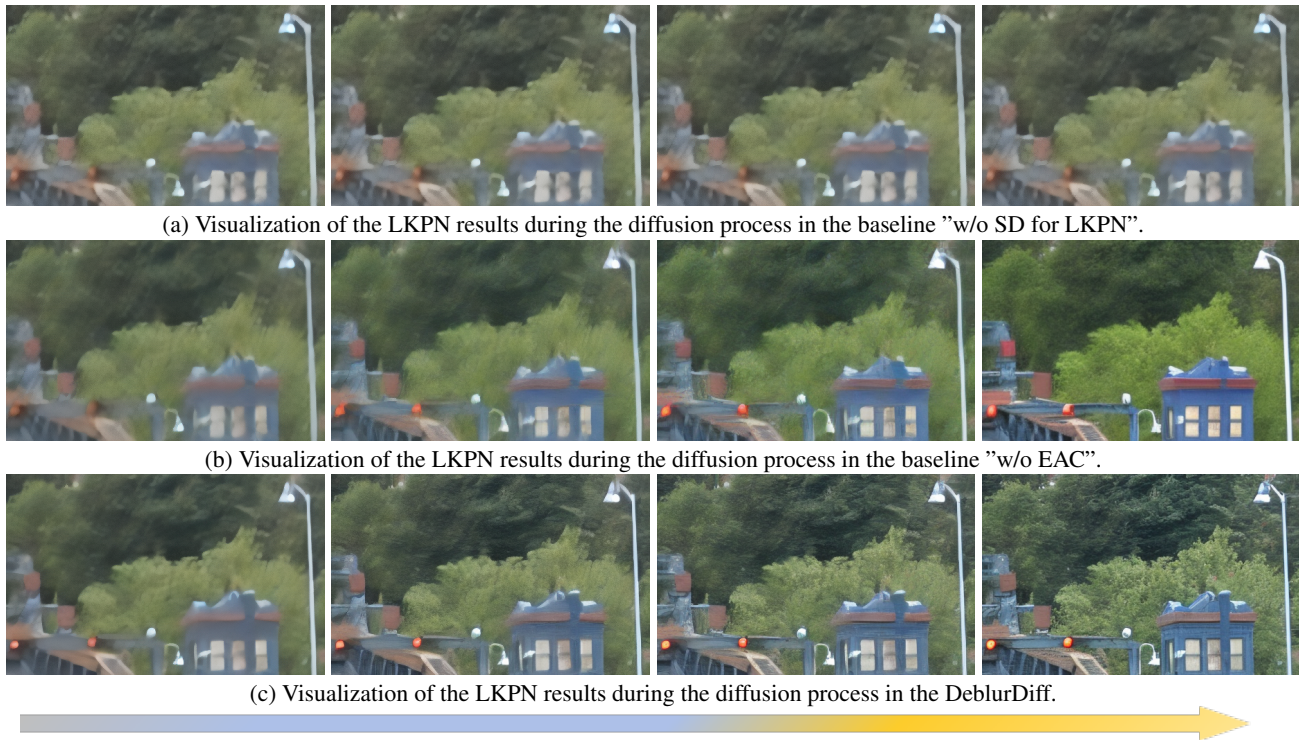


Figure 13. Iterative results of LKPN. The arrow represents the iterative diffusion process. To visualize this process, we decode the features deblurred by the LKPN to the image space using the VAE decoder in each time step.



Figure 14. Effectiveness of the proposed DeblurDiff on image deblurring. ControlNet struggles to recover clear structures due to the lack of explicit structural guidance, resulting in blurred outputs. Without the Stable Diffusion (SD) priors (referred to as w/o SD for LKPN), the LKPN fails to leverage intermediate clear priors for deblurring, leading to artifacts and inconsistencies in the generated results. When the LKPN directly predicts the deblurred result without using EAC (referred to as w/o EAC), the outputs tend to be overly smooth, losing important details and structural information. In contrast, our method effectively recovers sharp structures and fine details while preserving the input information. By leveraging intermediate clear priors from the diffusion process and adaptively estimating spatially variant kernels through EAC, our approach achieves better deblurring performance, generating visually appealing and realistic results.

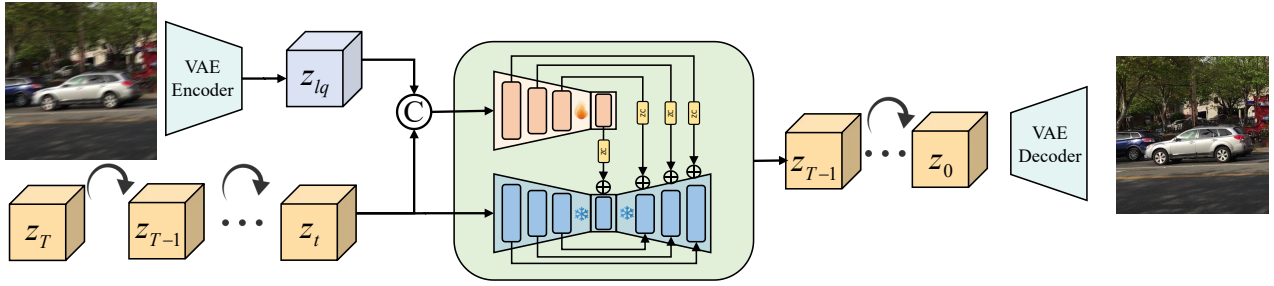


Figure 15. Overall architecture of ControlNet.

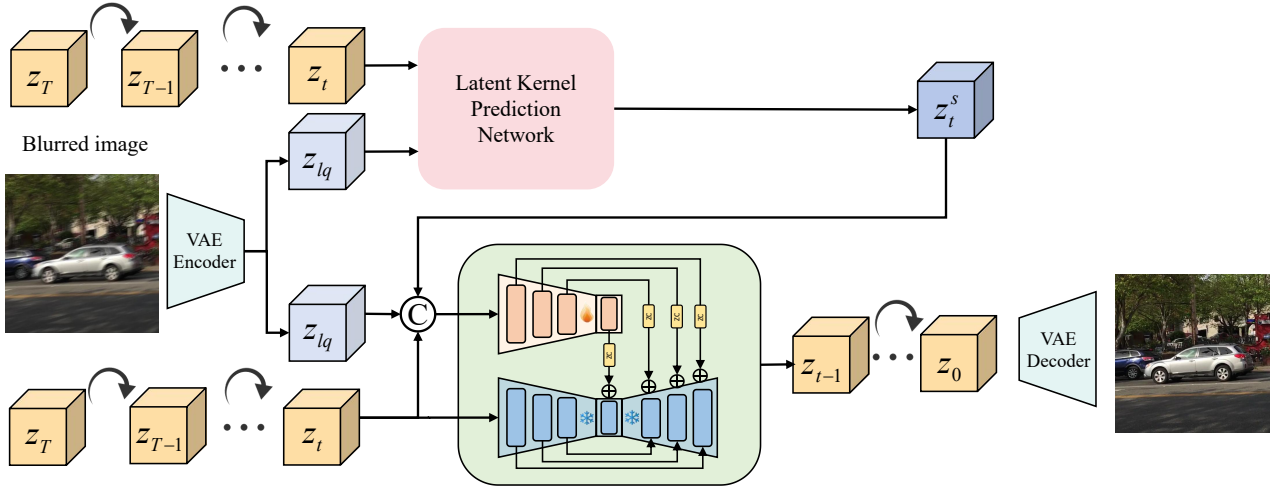


Figure 16. Overall architecture of the baseline "without EAC".

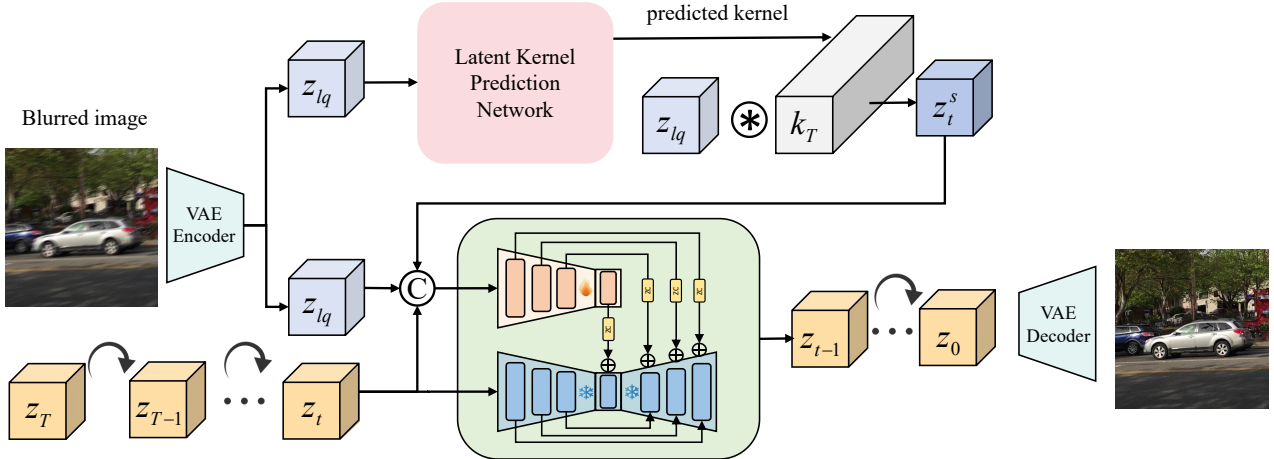


Figure 17. Overall architecture of the baseline "without SD".

E. Qualitative Comparisons.

In this section, we provide more visual comparisons of the proposed method with state-of-the-art ones on both synthetic and real-world benchmarks in Figures 18 to 21

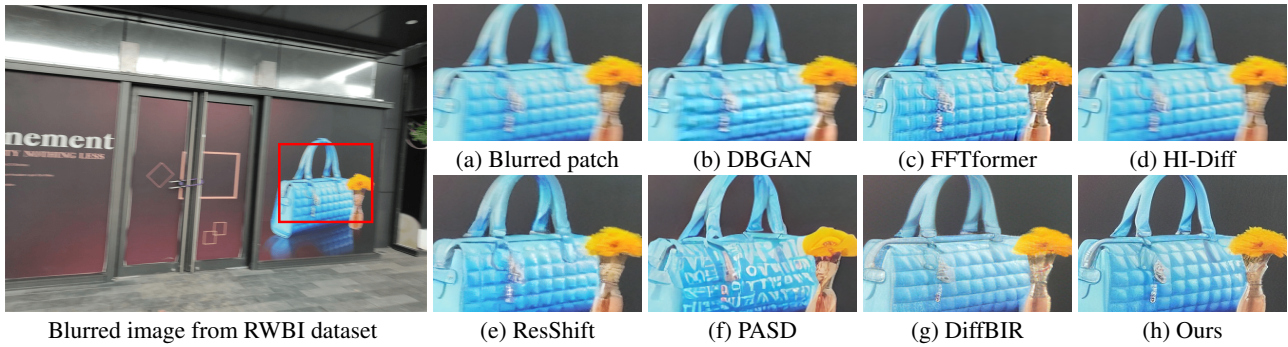


Figure 18. Visual comparison with state-of-the-art image deblurring methods. (b) to (g) fail to preserve the input information well while deblurring. In contrast our method generates clear results while effectively retaining the input information.

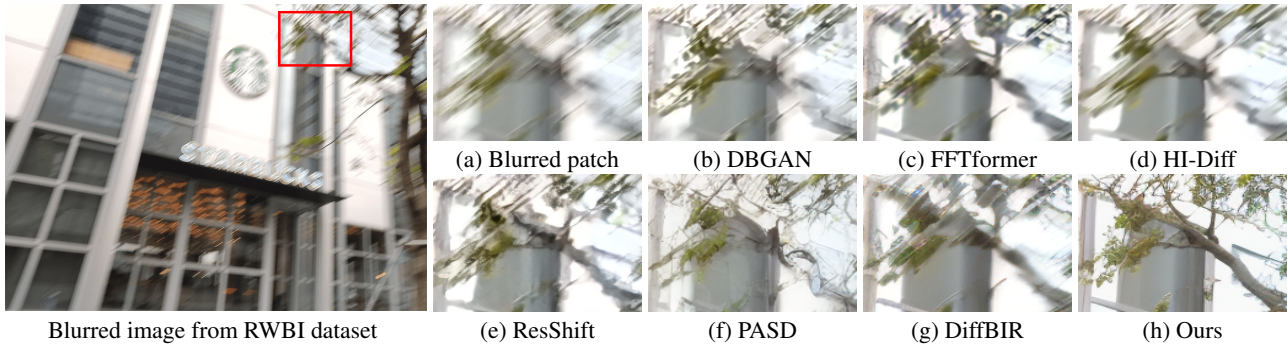


Figure 19. Visual comparison with state-of-the-art image deblurring methods. The deblurred results in (b)-(g) still contain significant blur effects. The proposed method generates a clearer image, where the structure of the branches and the leaves are much clearer.

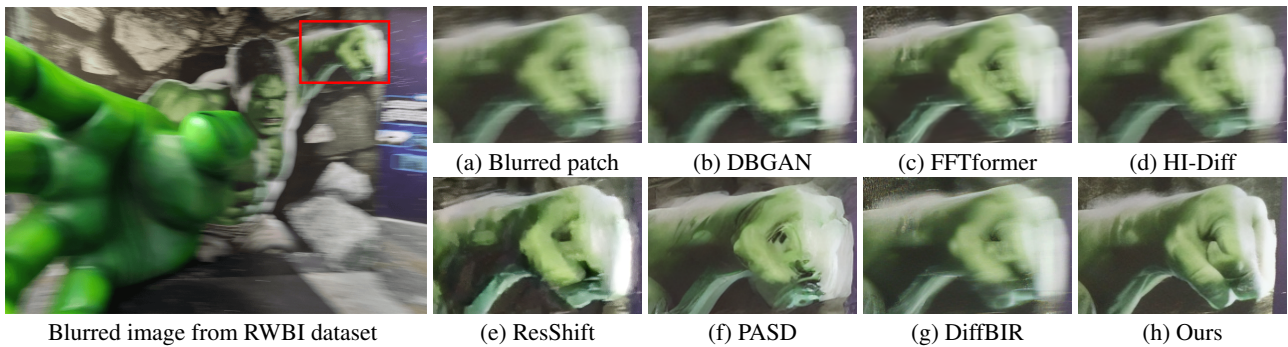


Figure 20. Visual comparison with state-of-the-art image deblurring methods. (b) to (g) leave severe artifacts. In contrast, our method generates a clear and realistic result.

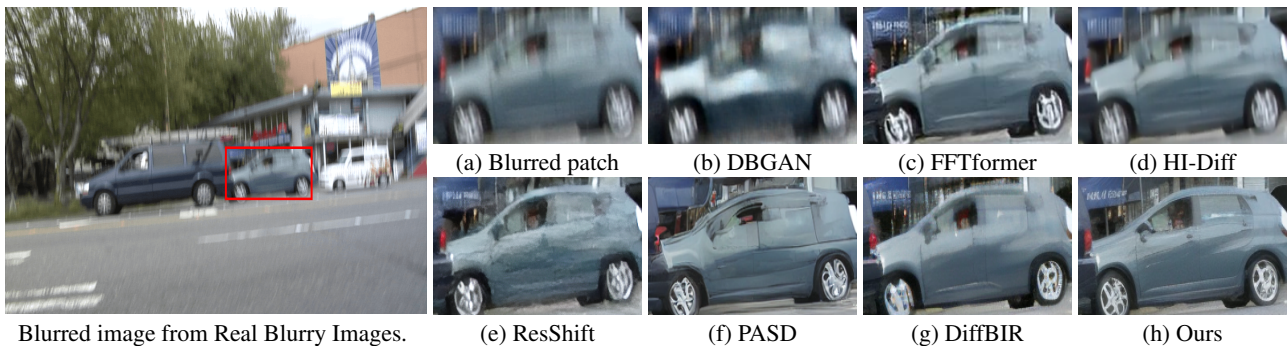


Figure 21. Visual comparison with state-of-the-art image deblurring methods. The structures in the results restored by methods (b) to (g) are all distorted. In contrast, the structures in our results are clear and accurate.